Physico-chemical characterization of the blooming of Irganox 1076® antioxidant onto the surface of a silane-crosslinked polyethylene

Anne Xu, Sébastien Roland, Xavier Colin*

PIMM, Arts et Metiers Institute of Technology, CNRS, CNAM, HESAM University, 151 Boulevard de L'Hopital, 75013, Paris, France

A B S T R A C T

This study aims at investigating the blooming of Irganox 1076® onto the surface of a silane-crosslinked polyethylene. Preliminary studies on the commercial Irganox 1076® powder enabled to identify its crystalline structure and determine its main physico-chemical properties (characteristic IR absorption bands, melting properties, etc.). Then, the behaviour of Irganox 1076® in silane-grafted polyethylene was studied. Several films containing a concentration of Irganox 1076® ranged between 0.1 wt% and 2.1 wt% were characterized with FTIR spectroscopy and DSC. A peculiar attention was paid to the phase separation within the polymer bulk and the blooming of the antioxidant onto the polymer film surface. Then, this methodology was transposed to an industrial silane-crosslinked polyethylene containing at least 1 wt% of Irganox 1076® as in-service protective antioxidant. For this latter, optical microscopy was of great help for monitoring the blooming of Irganox 1076® onto the polymer film surface. In addition, the polymorphism phenomenon of Irganox 1076® was revealed by FTIR spectroscopy and DSC after thermal treatment at 70 °C under vacuum.

Keywords:
Crosslinked polyethylene
Phenolic antioxidant
Phase separation
Blooming
Crystallization
Polymorphism

1. Introduction

Polyethylene (PE) is a widely used material and one of the most popular materials in engineering, as it is easily available at a relatively low cost, easily processable, relatively light and flexible, with good chemical resistance and non-toxic [1,2]. Polyethylene is a linear polymer belonging to the polyolefin family which can be easily shaped and reshaped, through modification or process conditions, into cables, pipes or films. This polymer is also well known to be an excellent dielectric material. For this reason, it is commonly used as an insulation material in power cables [3]. However, due to its low melting point, its maximum service temperature is generally limited to 55 °C [3–7]. In order to extend its range of use and improve its long-term mechanical properties at higher temperatures (typically up to 90 °C), this polymer can be crosslinked.

Crosslinking is a process of creating covalent bonds between polymer chains, i.e. leading to the formation of a three dimensional macromolecular structure. This modification of structure is generally chemically achieved through ionizing radiation (using gamma or electron beam), peroxide additives (at high temperature), or silane grafts along the polymer chain. Silane-crosslinking has recently gained much attention due the many advantages it can offer, such as its easy processing, its low cost and low capital investment [8–10], but also the favourable thermomechanical properties of the resulting material [11]. This crosslinking method consists of a two-step process: i) Grafting of silane side groups (named Si-OR, where R is an alkyl group) on polyethylene chains; ii) Transformation of silane into silanol side groups (Si–OH) by hydrolysis in order to form intermolecular siloxane junctions (Si–O–Si) by condensation.

As any hydrocarbon polymer, crosslinked polyethylene (XLPE) is sensitive to oxidation, which can be initiated by exposure to high temperature [12–16], ionizing radiations [17–20], UV-light [21–23] or radical reagents in aqueous chemical solutions [24–27]. Oxidative degradation is susceptible to occur at all stages of the polymer lifetime (i.e., synthesis, storage, processing, and in-service), and results on irreversible modifications of the polymer chemical composition. These chemical modifications commonly lead to a general loss of the polymer macroscopic properties (e.g., mechanical and dielectric properties), which can lead *in fine* to the material failure.

In order to protect them against oxidation, a small content of antioxidants (named AO) is generally incorporated into hydrocarbon polymers. Thus, many types of antioxidants have been

* Corresponding author.
E-mail address: xavier.colin@ensam.eu (X. Colin).

developed for their lifetime extension. They are organic molecules typically containing at least one of the following chemical functions: phenol, sulfide, amine, and phosphite [28–30], which are able to easily react with intermediate oxidation products, such as hydroperoxides and radicals, in order to significantly delay and slow down the oxidation kinetics. Contrarily to polyolefins, antioxidants are relatively polar molecules. Thus, their solubility threshold in PE is quite low. In addition, antioxidants are only soluble in the amorphous phase of semi-crystalline polymers. Indeed, the overall solubility threshold of antioxidants is a decreasing function of the polymer crystallinity ratio [31]. Typically, much less than 1 wt% of antioxidants is incorporated into semi-crystalline polymers, while between 1 and 2 wt% is typically used for protecting rubbers [28,30,32].

Antioxidants are incorporated into hydrocarbon polymers during the processing operation in melt state (i.e., at high temperature). At these temperatures, antioxidants are usually highly soluble in polymers. However, during cooling, as the solubility is a decreasing function of temperature, the polymer can become rapidly supersaturated in antioxidants. This excessive content of antioxidants can lead to a phase separation with crystallization of antioxidant nodules within the polymer bulk, but also to a surface segregation (through exudation) with crystallization of different antioxidant structures on the polymer sample surface (called blooming effect) [31–34]. In such a case, the material could be seen as a biphasic system consisting of an AO fully saturated polymer matrix containing a separated and more or less dispersed pure AO phase [35]. In addition, in semi-crystalline polymers, as antioxidants are only soluble in the amorphous phase, a release of the antioxidants towards the amorphous areas is typically observed during cooling, leading to a heterogeneous distribution of additives in the polymer bulk [36].

When considering crystallization of organic compounds, a ubiquitous issue encountered is polymorphism. Polymorphism phenomenon can be defined as the ability of a crystalline phase to exist in more than one lattice structure, and concerns many antioxidants [33,37–39]. Formation of a polymorph depends on several factors such as the polymorph stability, but also the general conditions of the crystallization process (i.e., use of solvent, temperature, level of supersaturation, etc.). Due to their different crystalline structures, polymorphs may have different properties, e.g., different melting points, dissolution rates, optical properties, reactivities in solid-state, etc.

Octadecyl-3,5-di-tert-butyl-4-hydroxyhydrocinnamate, well known as Irganox 1076® (see Fig. 1), is a commercial phenolic antioxidant commonly used for the stabilization of polyolefins in a wide range of applications (e.g. electrical cables insulation, biomedical devices, etc.). Only few information is available on the polymorphism phenomenon of this phenolic antioxidant. However, Molt and Ihlbrock [40] mentioned the existence of two different crystalline structures of Irganox 1076®, named “alpha” and “beta”, which could be distinguished using near infrared spectroscopy. More recently, Saunier et al. [33,41] mentioned the existence of four different crystalline structures for Irganox 1076®, among which three of them were obtained and isolated by recrystallization in different solvents.

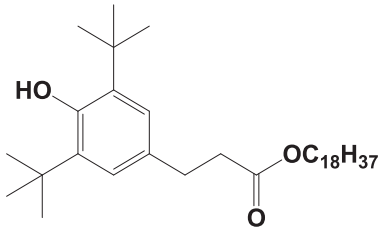

Fig. 1. Chemical structure of Irganox 1076®.

In this study, the behaviour of Irganox 1076® in silane-grafted polyethylene was investigated using FTIR spectroscopy and DSC analysis. A peculiar attention was paid to the phase separation within the polymer bulk and the blooming of the antioxidant onto the polymer sample surface. Then, the methodology was applied to an industrial silane-crosslinked polyethylene containing Irganox 1076® as in-service protective antioxidant. In addition, a thermal treatment was performed in soft conditions (typically at 70 °C under vacuum) to study the polymorphism stability of antioxidant crystals without inducing an undesired chemical degradation in polymer samples.

2. Materials and methods

2.1. Preparation of films of silane-grafted PE stabilized with Irganox 1076®

Irganox 1076® was supplied by Sigma Aldrich in the form of a white powder. Silane-grafted linear low-density polyethylene (named Si-g-LLDPE) pellets were gratefully provided by Nexans NRC, Lyon (France). The crystallinity ratio of this polymer is about 40%.

Si-g-LLDPE pellets were micronized using a FRITSCH Variable Speed Rotor Mill Pulverisette 14 in order to obtain a polymer powder having an average grain diameter of about a dozen of microns. It should be mentioned that the pellets contain a small quantity of storage phenolic antioxidants (mainly BHT and Irganox 1076®, identified by HPLC) which were not removed in order to protect the polymer against thermal oxidation during the micronization. It was checked by FTIR spectrometry that these storage antioxidants were not totally consumed after this operation preliminary to processing. Indeed, very small concentrations of antioxidants were detected in the resulting Si-g-LLDPE film (typically 0.1 wt%) in comparison with the additional concentration of AO introduced in the films (up to 2 wt%). However, the storage AO were considered for the calculation of the total concentration of AO in the stabilized Si-g-LLDPE films, thus inducing a small shift between the total concentrations of ester and phenol functions.

Thin Si-g-LLDPE films of 100–200 μm thick containing different concentrations of Irganox 1076® were obtained by mixing the Si-g-LLDPE and Irganox 1076® powders, then by hot-compressing the mixture at 150 °C under 200 bars pressure for 4 min with a Gibitre Instruments laboratory press. The additional concentration of Irganox 1076® was typically ranged between 0 and 2 wt%. All films were stored at ambient temperature in a desiccator containing silica gel before any physico-chemical characterization.

2.2. Films of silane-crosslinked PE stabilized with Irganox 1076®

Films of silane-crosslinked polyethylene (named Si-XLPE) of about 500 μm thick containing at least 1 wt% of Irganox 1076® were directly provided by Nexans. These films were also produced by hot-compression molding, and the crosslinking was performed by immersion of the films in water at 65 °C for 48 h. They were stored at ambient temperature in a desiccator containing silica gel before any physico-chemical characterization.

2.3. Thermal treatment

The stabilized polymer films were exposed at low temperature but above the melting point of Irganox 1076® (typically 70 °C) under vacuum in order to study the polymorphism stability of

antioxidant crystals without inducing an undesired chemical degradation in the polymer samples i.e., an antioxidant consumption by the polymer oxidation.

2.4. Fourier-transform infrared spectroscopy (FTIR)

FTIR spectra were recorded using a PerkinElmer FTIR Frontier spectrometer from 4000 to 650 cm^{-1} in Attenuated Total Reflectance (ATR) mode, or from 4000 to 400 cm^{-1} in transmission mode, after having averaged the 16 scans obtained with a minimum resolution of 4 cm^{-1}. In case of ATR mode, the analyses were performed with a diamond/ZnSe crystal.

The commercial Irganox 1076® powder was characterized by FTIR spectroscopy using three methods: in ATR mode without any prior preparation, in transmission mode using KBr discs, and in transmission mode using a liquid cell. For the second method, thin KBr discs were prepared by mixing 100 mg of KBr powder, with 0.3 mg−1 mg of Irganox 1076® powder. The resulting mixture was grinded into a fine powder using a mortar, then compressed for 5 min under 4 MPa. For the last method, the Irganox 1076® powder was dissolved in an organic solvent, and the resulting solution was poured in a sealed liquid cell with KBr windows, having an optical path length of 0.12 cm. The solvents used in this study were dichloromethane and cyclohexane.

The stabilized polymer films were characterized before and after thermal treatment by FTIR spectroscopy in both ATR and transmission modes without any prior preparation.

2.5. Differential scanning calorimetry (DSC)

DSC thermograms were recorded using a TA instrument DSC Q1000 calorimeter beforehand calibrated with an indium reference. Samples with a mass ranged between 5 mg and 8 mg were introduced in a closed standard aluminium pan to be analysed under a pure N_2 flow of 50 mL min^{-1} between - 50 °C and 100 °C with heating and cooling rates of 10 °C.min^{-1}.

2.6. Optical microscopy

The surface of the Si-XLPE films was examined before and after thermal treatment using a Zeiss Axio Imager 2 optical microscope in reflection mode with polarized light.

3. Results and discussion

3.1. Physico-chemical characterization of the Irganox 1076® powder

3.1.1. DSC analysis

The commercial Irganox 1076® powder was first analysed by DSC. The resulting thermograms obtained are given in Fig. 2. Different endothermic and exothermic peaks were observed. During the first heating ramp, between - 50 °C and 100 °C, a single endothermic peak was observed at 52 °C corresponding to the melting of the initial Irganox 1076® crystals. Then, during the cooling ramp up to - 50 °C, two exothermic peaks were observed: one at 3 °C and other at - 4 °C. Finally, during the last heating ramp up to 100 °C, three peaks were observed: a first endothermic peak at 6 °C followed immediately by an exothermic peak at 14 °C, then another endothermic peak at 52 °C.

According to literature, Irganox 1076® can crystallize under different structures [33,40,41]. Saunier et al. [41], for instance, mentioned the existence of four different crystalline structures that they called forms I, II, III, and IV. The commercially available structure, called form I by these authors, is characterized by the highest melting point. It is thus the most thermodynamically stable crystal. The endothermic peak observed at 52 °C during the first heating ramp in Fig. 2 corresponds well to the melting of this form I. In addition, the exothermic peak observed at 3 °C during the cooling ramp at 10 °C.min^{-1} corresponds to the recrystallization of Irganox 1076® into the metastable crystalline form IV. This latter structure is only stable at low temperature and is generally obtained by rapid cooling after melting [41]. Indeed, its melting peak observed at 6 °C during the second heating ramp was immediately followed by an exothermic peak of recrystallization into form I. The two other crystalline structures, called forms II and III in the literature, were not observed during these DSC experiments. In fact, forms I and IV seem to be monotropically related, the latter being the metastable form [33]. At the opposite, transformations into forms II and III are more complex and seem to involve enantiotropic transitions. For this reason, they cannot be discriminated using classical DSC experiments [41].

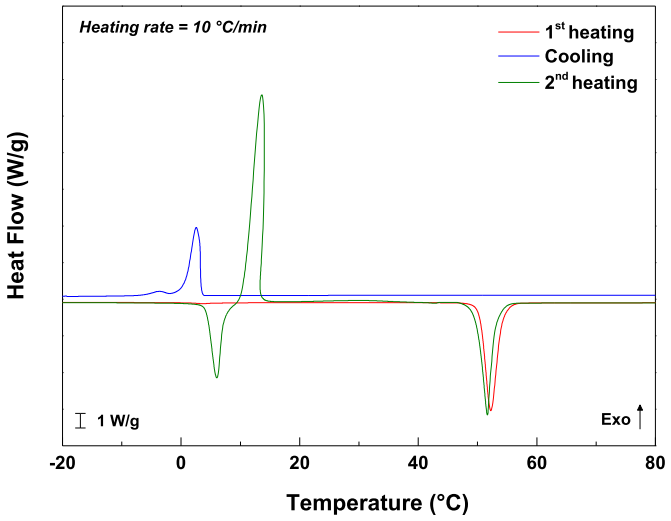

Fig. 2. DSC thermograms obtained for the commercial Irganox 1076® powder (between −50 °C and 100 °C, but only the interval between −20 °C and 80 °C is represented) with heating and cooling rates of 10 °C.min^{-1}.

As previously said, the so-called form I is the commercially available crystalline structure with the highest melting point. Its melting properties found by DSC are the following: $T_m = 52.0 \pm 0.4$ °C and $\Delta H_m = 119 \pm 1$ J g^{-1}. These values are quite consistent with literature data [41].

3.1.2. FTIR spectroscopy

3.1.2.1. In crystalline state. The commercial Irganox 1076® powder was then analysed by FTIR spectroscopy in ATR mode. As shown in Fig. 3, the characteristic IR absorption bands of the phenol and ester functions of Irganox 1076® were observed at 3639 cm^{-1} and 1733 cm^{-1}, respectively. The bands of CH_3 groups at 2953 cm^{-1}, and those of aromatic ring at 3002 cm^{-1}, 3070 cm^{-1} and 870 cm^{-1}, were also clearly distinguished. Table 1 summarizes the different IR absorption bands of the Irganox 1076® powder and their attributions.

According to literature, the different polymorphic forms of Irganox 1076® can be distinguished using FTIR spectroscopy [33,40,41]. Here, only one IR absorption band at 3639 cm^{-1} was observed for the phenol function which, according to Saunier et al. [33], corresponds to the phenol function of form I. Indeed, according to these authors, the phenol bands of forms II and III are assumed to be observed at lower wavenumbers.

The commercial Irganox 1076® powder was also characterized through FTIR spectroscopy in transmission mode using KBr discs.

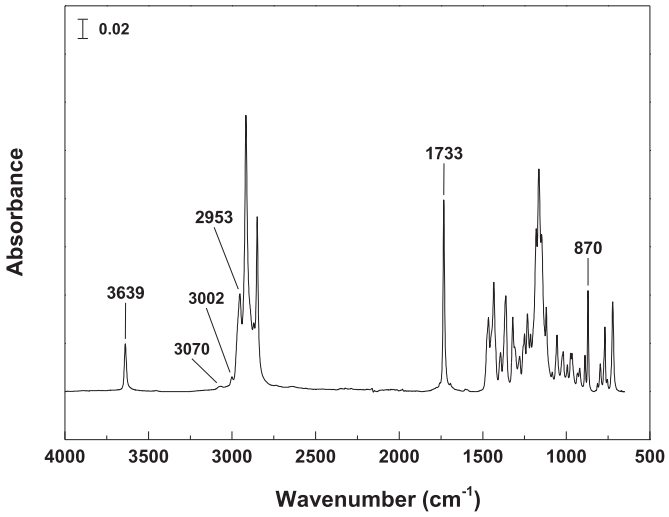

Fig. 3. FTIR spectrum obtained in ATR mode for the commercial Irganox 1076® powder.

Table 1
Attribution of the IR absorption bands of the commercial Irganox 1076® powder [33,42,43].

Wavenumber (cm^{-1})	Attribution
3639	O–H stretching (phenol)
3002	C–H stretching (aromatic)
3070	
2953	C–H stretching (CH_3)
1733	C=O stretching (ester)
1000–1400	C–O stretching (ester and phenol)
870	=C–H bending (aromatic)

As previously said, KBr discs with increasing concentration in Irganox 1076® from 0.3 wt% ($\approx 1.7 \times 10^{-2}$ mol L^{-1}) to 1 wt% ($\approx 5.5 \times 10^{-2}$ mol L^{-1}) were elaborated. The hydroxyl and carbonyl regions of the FTIR spectra, normalized with the KBr disc thickness (noted "e"), are shown in Fig. 4a.

The normalized absorbance of the IR absorption bands at 3640 cm^{-1} (for phenol) and 1735 cm^{-1} (for ester) were plotted against the nominal concentration of the respective chemical function. The resulting graphs are shown in Fig. 4b and c, respectively. In this concentration range, the material under study seems to obey the Beer-Lambert's law, which can be written as follows:

$$A = \varepsilon.e.C \quad \text{(Eq. 1)}$$

Where A is the absorbance, e the sample thickness (cm), C the concentration of the absorbing species (mol.L^{-1}) and ε the molar extinction coefficient (L.mol^{-1} cm^{-1}).

The molar extinction coefficients of ester and phenol functions of the Irganox 1076® crystal were found to be equal to 493 ± 12 L mol^{-1} cm^{-1} and 208 ± 5 L mol^{-1} cm^{-1}, respectively. The former is quite consistent with the values reported for ester functions in the literature [44–46]. In contrast, the value obtained for the phenol function seems to be too high when compared to the values reported in the literature for hydroxyl functions such as hydroperoxides and alcohols, which are generally ranged between 70 and 90 L mol^{-1} cm^{-1} [43,45]. However, as Irganox 1076® was characterized in its crystalline form, the high value of the molar extinction coefficient found for the phenol function could be due to intense interactions between antioxidant molecules, such as hydrogen bonding. Indeed, in a previous paper, Carlsson et Wiles [47] found a molar extinction coefficient of 150 ± 15 L mol^{-1} cm^{-1} for the hydrogen-bonded OH function of t-butyl alcohol.

3.1.2.2. In dispersed state. The commercial Irganox 1076® powder was also dissolved in two organic solvents to be analysed in dispersed state by FTIR spectroscopy in transmission mode. On the one hand, the experiment was performed in cyclohexane, which is an apolar solvent. This solvent was chosen because its solubility parameter ($\delta = 16.7$ $MPa^{1/2}$ [48]) is close to that of PE which, according to literature, is typically ranged between 15.8 and 17.1 $MPa^{1/2}$ [48]. It is thus expected that cyclohexane establishes similar intermolecular interactions than PE with Irganox 1076® molecules. A series of solutions of Irganox 1076® in cyclohexane, with concentrations ranged between 0.05 wt% ($\approx 1 \times 10^{-3}$ mol L^{-1}) and 0.7 wt% ($\approx 1 \times 10^{-2}$ mol L^{-1}), was prepared and analysed by FTIR spectroscopy using a liquid cell. The corresponding spectra were subtracted from the solvent spectrum in order to only observe and analyse the IR absorption bands of Irganox 1076®. An example of FTIR spectra is shown in Fig. 5. The bands of phenol and ester functions were observed at 3651 cm^{-1} and 1742 cm^{-1}, respectively (i.e., at positions slightly higher than the previous ones observed for the Irganox 1076® crystal).

On the other hand, the same experiment was performed in a more polar solvent: dichloromethane (solubility parameter $\delta = 19.9$ $MPa^{1/2}$ [29]). As previously, a series of solutions of Irganox 1076® in dichloromethane, with concentrations ranged between 0.04 wt% ($\approx 1 \times 10^{-3}$ mol L^{-1}) and 1.2 wt% ($\approx 3 \times 10^{-2}$ mol L^{-1}), was prepared and analysed by FTIR spectroscopy using a liquid cell. An example of FTIR spectra is also shown in Fig. 5. Contrarily to cyclohexane, the bands of phenol and ester functions were observed at 3637 cm^{-1} and 1726 cm^{-1}, respectively (i.e., at positions slightly lower than the previous ones observed for the Irganox 1076® crystal). In addition, these bands were much broader in dichloromethane than in cyclohexane. Examples of FTIR spectrum of Irganox 1076® obtained in three different chemical environments are overlaid in Fig. 5.

Table 2 compiles the positions of IR absorption bands obtained for the two chemical functions of Irganox 1076® under study in different chemical environments.

Regarding these experimental results, it seems that the chemical environment has a significant influence on both the position and the width of IR absorption bands of the two chemical functions under study. As previously said, dichloromethane and cyclohexane have quite different polarities. The former can be considered as a moderately polar solvent, while the latter is clearly an apolar solvent. In contrast, Irganox 1076® is assumed to be a much higher polar molecule. Van Krevelen and Te Nijenhuis reported solubility parameters of 24.1 $MPa^{1/2}$ for phenol and 22.7 $MPa^{1/2}$ for m-cresol (a phenol derivative) [48].

Indeed, the position of the IR absorption bands of ester and phenol functions are found to be lower in a polar solvent (i.e., a good solvent) than in an apolar solvent. This difference could be due to the nature and strength of the intermolecular interactions involved between the solvent and antioxidant molecules. Indeed, if assuming its complete dissolution in dichloromethane, Irganox 1076® is capable of establishing intense interactions with dichloromethane, such as H-bonds involving O–H stretching vibration. In this case, a red-shift (i.e., a shift towards lower wavenumbers) accompanied with a broadening of the IR absorption bands is generally observed due to a weakening of the O–H bond [37,49]. At the opposite, much less intense interactions (only van der Waals type) are expected to be involved between Irganox 1076® and cyclohexane.

In solid state (crystalline AO powder), intermediate positions are found for the IR absorption bands of the two chemical functions of

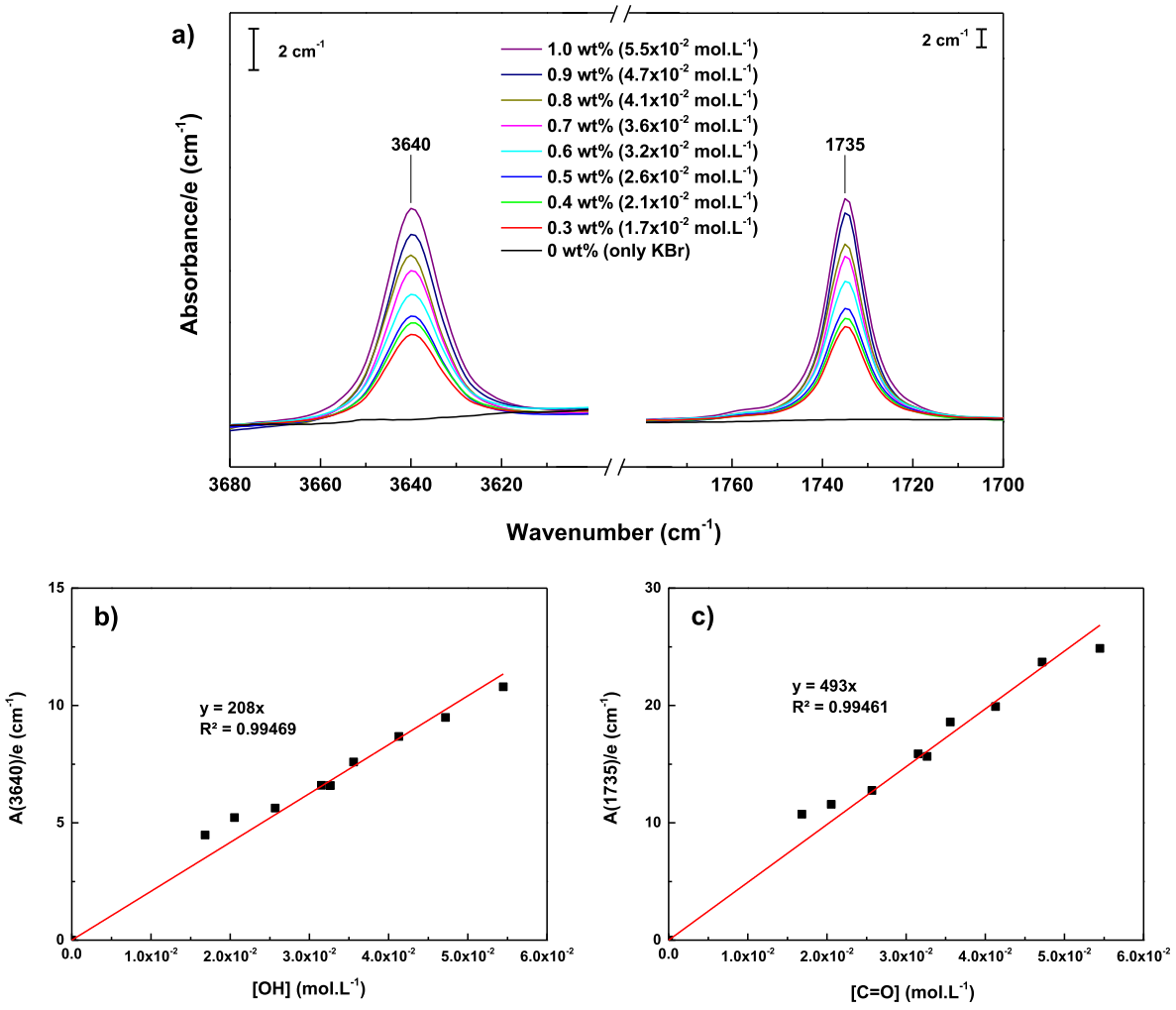

Fig. 4. a) Normalized hydroxyl and carbonyl regions of the FTIR spectra obtained in transmission mode using KBr discs with increasing the concentration in Irganox 1076® powder, b) Calibration curve of A (3640)/e against [OH], and c) Calibration curve of A (1735)/e against [C═O].

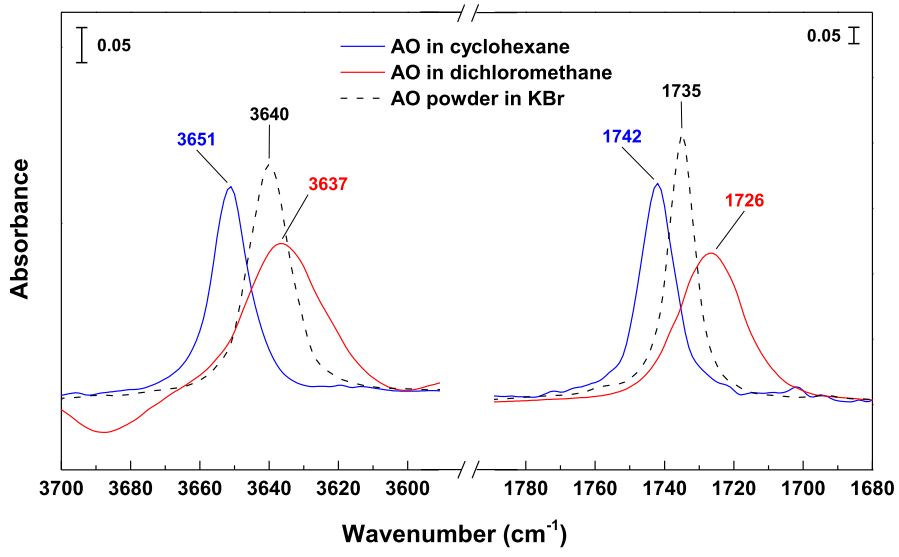

Fig. 5. Hydroxyl and carbonyl regions of the FTIR spectra obtained in transmission mode for solutions of Irganox 1076® (with a concentration of 1×10^{-2} mol L^{-1}) in cyclohexane and dichloromethane, and for the Irganox 1076® powder in KBr pellet.

Table 2
Positions of IR absorption bands and molar extinction coefficients obtained for phenol (OH) and ester (C=O) functions in different chemical environments using FTIR in transmission mode.

FTIR	Phenol		Ester	
	ν_{OH} (cm^{-1})	ε_{phenol} ($L.mol^{-1}.cm^{-1}$)	$\nu_{C=O}$ (cm^{-1})	ε_{ester} ($L.mol^{-1}.cm^{-1}$)
Solution of Irganox 1076® in cyclohexane	3650	/	1742	/
Solution of Irganox 1076® in dichloromethane	3637	/	1726	/
KBr discs with Irganox 1076® powder	3640	208 ± 5	1735	493 ± 12

Irganox 1076®. Undoubtedly, H-bonding is also involved between Irganox 1076® molecules, but it is presumably slightly weakened by the steric hindrance all around the phenol function (protected by two tert-butyl groups, see Fig. 1).

3.2. Physico-chemical characterization of stabilized polymer films

3.2.1. Characterization of the polymer film surface

3.2.1.1. Si-g-LLDPE films. Si-g-LLDPE films stabilized with different concentrations of Irganox 1076®, typically ranged between 0.1 wt% ($\approx 2.0 \times 10^{-3}$ mol L^{-1}) and 2.1 wt% ($\approx 3.7 \times 10^{-2}$ mol L^{-1}), were first characterized on their surface by FTIR spectroscopy in ATR mode.

The hydroxyl and carbonyl regions of the FTIR spectra obtained in ATR mode are given in Fig. 6a. In both regions, no IR absorption band of Irganox 1076® was observed for concentrations typically below 0.9 wt% ($\approx 1.6 \times 10^{-2}$ mol L^{-1}) of Irganox 1076® in PE. Above this critical value, two IR absorption bands, assigned to phenol and ester functions, were observed at 3639 cm^{-1} and 1733 cm^{-1}, respectively, and seemed to increase with the AO concentration. The positions of these bands correspond well to those of the crystalline form I of Irganox 1076® (see Table 2), which means that the antioxidant detected onto the polymer film surface is in the crystalline form I.

At this stage of investigation, it is important to remind that, when using FTIR in ATR mode, mainly the sample surface will be analysed, unlike in transmission mode where the whole sample thickness is analysed. Indeed, the penetration depth D_p of the IR radiation in ATR mode depends on several factors: wavelength, refractive indices of the ATR crystal and sample, and angle of the entering light beam. It can be determined using the following equation [37,51,52]:

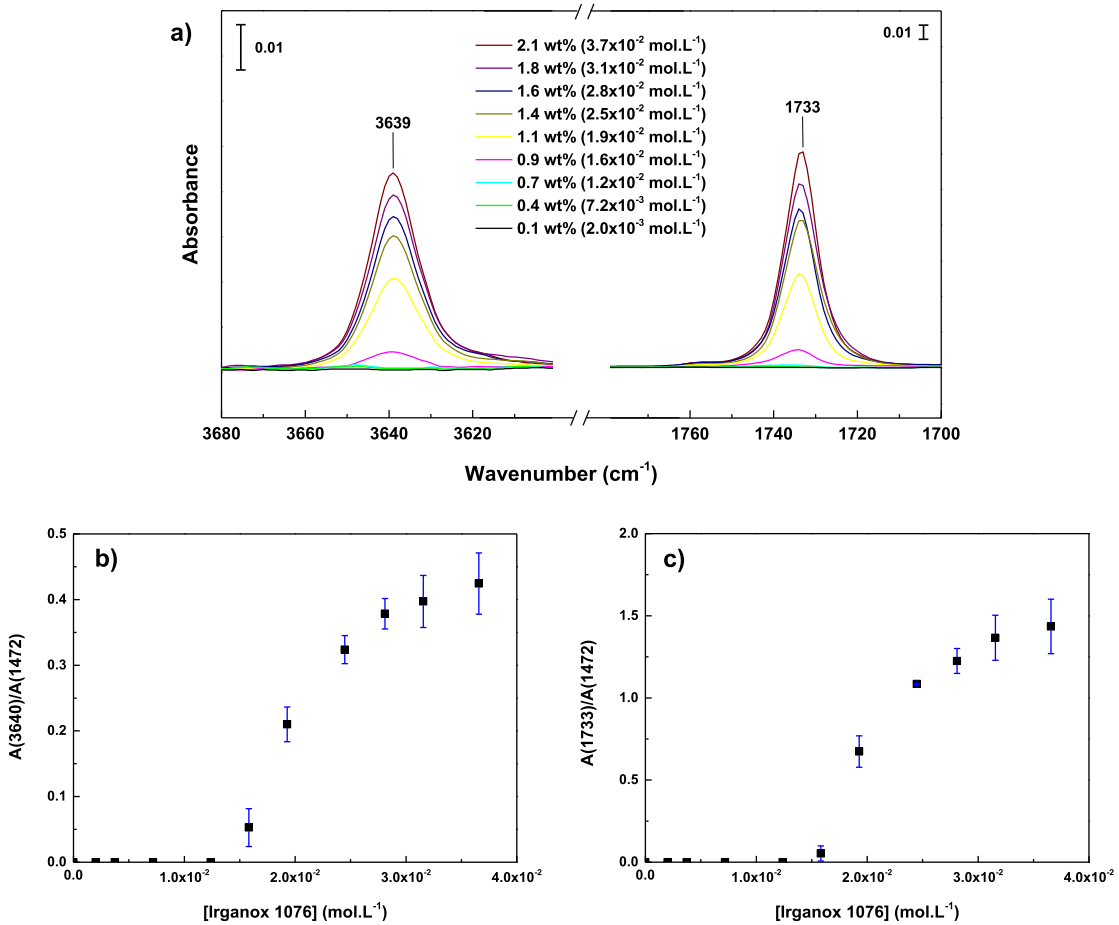

Fig. 6. a) Hydroxyl and carbonyl regions of the FTIR spectra obtained in ATR mode for the Si-g-LLDPE films stabilized with an increasing concentration in Irganox 1076®, b) Absorbance ratios against concentration of Irganox 1076® for phenol, and c) ester functions.

$$D_p = \frac{\lambda}{2\pi n_1 \left(\sin^2(\theta) - \left(\frac{n_2}{n_1} \right)^2 \right)^{1/2}} \quad \text{(Eq. 2)}$$

where λ is the wavelength of the IR beam, θ is its incidence angle ($\theta = 45°$), and n_1 and n_2 are the refractive indexes of the ATR crystal and polymer sample, respectively. According to literature, the refractive index is typically ranged between 1.47 and 1.52 for PE [53–55], and about 2.40 for a diamond ATR crystal [56].

The application of Eq. (2) leads to D_p values ranging between 0.2 μm and 1.3 μm for PE samples, depending on the wavenumber (from 4000 to 650 cm^{-1}). As a consequence, mainly the sample surface is analysed when FTIR spectroscopy is used in ATR mode and, for a given wavenumber, D_p takes a constant value.

To better observe the concentration changes in the two bands of the AO, their absorbance was normalized with the absorbance of the CH_2 scissoring vibrations of the PE crystalline phase at 1472 cm^{-1} [50]. The absorbance ratio were then plotted against the concentration of Irganox 1076® in PE in Fig. 6b and c, respectively. It can be observed that, for both phenol and ester functions, the absorbance ratio does not vary and is practically zero for AO concentrations below 0.9 wt% ($\approx 1.6 \times 10^{-2}$ mol L^{-1}). Then, as the concentration of antioxidant increases, the absorbance ratio starts to increase. In addition, above approximately 3×10^{-2} mol L^{-1}, the concentration changes in the absorbance ratio slow down to quickly tend towards an asymptotic value.

These FTIR results obtained in ATR mode can be interpreted as follows. For concentration of Irganox 1076® below 0.9 wt% ($\approx 1.6 \times 10^{-2}$ mol L^{-1}), no antioxidant has been detected on the polymer film surface, which means that no exudation of Irganox 1076® has occurred or at least, the phenomenon extend is clearly too small to be detected using this technique. For an AO concentration equal and higher than this critical value, antioxidant starts to be detected and, as its concentration increases, the amount of antioxidant crystals detected on the polymer film surface increases. This observation means that the blooming of Irganox 1076® onto the polymer film surface is detected above typically 0.9 wt% ($\approx 1.6 \times 10^{-2}$ mol L^{-1}) and, as the concentration of antioxidants increases, the amount of exuded antioxidants increases. Thus, at term, a pure thin layer of crystalline antioxidants is formed on the polymer film surface, and this layer significantly reduces the penetration of IR radiation into the depth of polymer film (screen effect). This effect could explain the appearance of a saturation plateau for the concentration changes of the absorbance ratio, for both phenol and ester functions, as evidenced in Fig. 6b and c, respectively.

3.2.1.2. Si-XLPE film before and after thermal treatment. The surface of Si-XLPE film stabilized with at least 1 wt% ($\approx 1.7 \times 10^{-2}$ mol L^{-1}) of Irganox 1076® was characterized before and after one week of thermal treatment at 70 °C under vacuum. It should be highlighted that, as for Si-g-LLDPE, a phase separation with AO blooming was initially detected on the Si-XLPE film surface using FTIR spectroscopy in ATR mode, but also using optical microscopy in reflection mode. As an example, Fig. 7a shows the presence of crystals of various sizes (from few microns to a dozen of microns) which, according to FTIR results (see Fig. 8), should correspond to the (crystalline) form I of Irganox 1076.

Then, after one week of thermal treatment at 70 °C under vacuum, some interesting changes were observed on the Si-XLPE film surface, more precisely, concerning the crystalline structure of antioxidants. Indeed, as shown in Fig. 7b, the formation of needle-shaped crystals was evidenced using optical microscopy in reflection mode.

The polymer film surface was then analysed using FTIR spectroscopy in ATR mode. The hydroxyl and carbonyl regions of the FTIR spectra obtained before and after thermal treatment are given in Fig. 8. It can be seen that the IR absorption bands of both phenol and ester functions are shifted towards lower wavenumbers after thermal treatment, compared to untreated sample.

This wavenumber shift can be explained by a change in the crystalline structure of antioxidant (polymorphism), as already evidenced by several authors in the literature [33,40]. In particular, Saunier et al. [33] observed the formation of needle-shaped crystals on the surface of a medical device made of polymer, that they have attributed to the crystalline form III of Irganox 1076®. They showed that this new crystalline form has a specific IR signature, differing tremendously from form I. Indeed, the IR absorption band of the phenol function of form III is located at 3612 cm^{-1} (against 3639 cm^{-1} for form I). The present study confirms this attribution, but also brings an additional information concerning the IR absorption band of the ester function: it is located at 1723 cm^{-1} for form III (against 1733 cm^{-1} for form I).

Thus, the thermal treatment at 70 °C under vacuum causes the formation of a new crystalline structure (form III) of Irganox 1076® on the polymer film surface. Indeed, Irganox 1076® is a molecule which can undergo polymorphism and, according to literature, at least four different crystalline structures can exist [33,40,41]. At 70 °C, above the melting point (51 °C) of the form I of Irganox 1076, the thermal treatment induces the melting of AO crystals. Then, during the cooling down to ambient temperature, the antioxidants exuded on the polymer film surface where they recrystallized under a new structure (form III).

3.2.2. Characterization of the polymer bulk

3.2.2.1. Si-g-LLDPE films. Si-g-LLDPE films stabilized with different concentrations of Irganox 1076®, typically ranged between 0.1 wt%

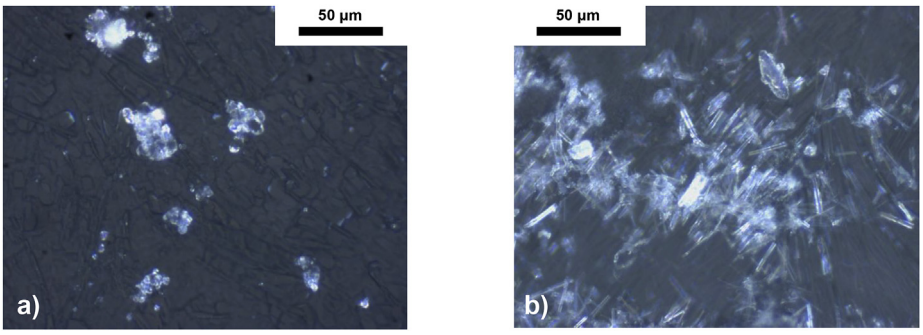

Fig. 7. Micrographs of the surface of a Si-XLPE film stabilized with Irganox 1076®: a) before, and b) after one week of thermal treatment at 70 °C under vacuum (with G = 500x).

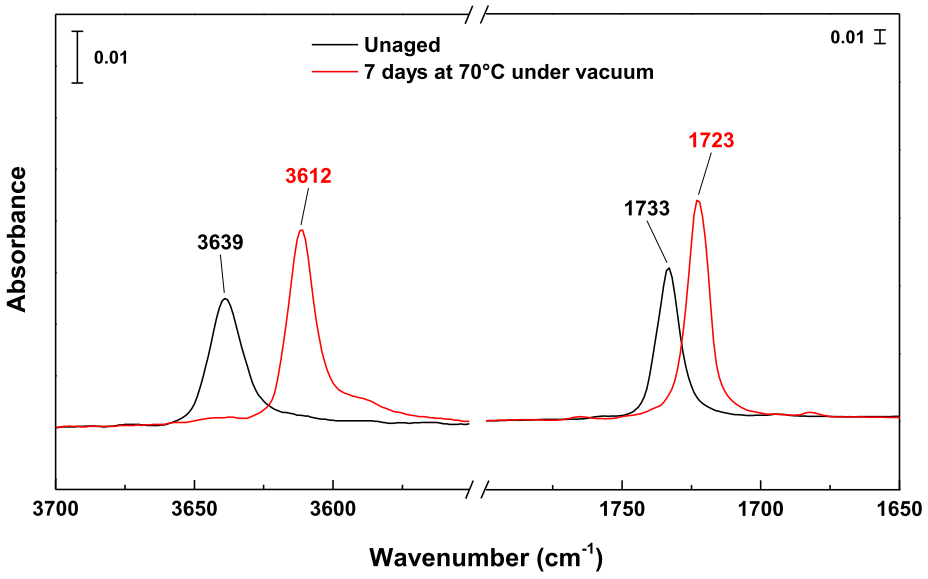

Fig. 8. Hydroxyl and carbonyl regions of the FTIR spectra obtained in ATR mode for the Si-XLPE film stabilized with Irganox 1076®, before and after one week of thermal treatment at 70 °C under vacuum.

($\approx 2.0 \times 10^{-3}$ mol L^{-1}) and 2.1 wt% ($\approx 3.7 \times 10^{-2}$ mol L^{-1}), were also characterized by FTIR spectroscopy in transmission mode and DSC in order to investigate the polymer bulk.

The hydroxyl and carbonyl regions of the FTIR spectra obtained in transmission mode, normalized with the thickness of the polymer films, are given in Fig. 9a. It should be mentioned the presence of an IR band at 3605 cm^{-1} for all the studied samples. In fact, according to literature [57–59], when the PE samples are sufficiently thick, two IR bands around 3605 cm^{-1} and 3645 cm^{-1} can be observed. According to Nielson et al. [57,59], the presence of these IR bands in PE is due to two-phonon combinations of CH_2 asymmetric stretching and rocking modes, i.e. to PE itself.

Concerning the antioxidant, it can be seen that the IR absorption bands of both phenol and ester functions are slightly shifted towards higher wavenumbers (at 3648 cm^{-1} and 1740 cm^{-1}, respectively), in comparison with the previous positions of bands detected in ATR mode and assigned to the crystalline form I of Irganox 1076® (at 3639 cm^{-1} and 1733 cm^{-1}, respectively). It is noteworthy that these wavenumbers are relatively close to the ones observed for solutions of Irganox 1076® in cyclohexane (see Table 2), which is an apolar solvent having almost the same solubility parameter than PE. It can be thus concluded that, as long as its concentration in Si-g-LLDPE films is low enough, Irganox 1076® is well dissolved in Si-g-LLDPE films and thus, intense intermolecular interactions between AO molecules (such as in AO crystals) are unlikely to occur. In other words, the IR absorption bands of the phenol function at 3648 cm^{-1} and ester function at 1740 cm^{-1} can be assigned to Irganox 1076® in a dissociated state in the polymer bulk. This conclusion is consistent with the previous FTIR results obtained in ATR mode for which the formation of AO crystals started to be detected on the polymer film surface above a critical concentration of about 0.9 wt% ($\approx 1.6 \times 10^{-2}$ mol L^{-1}).

The resulting normalized absorbance of the IR absorption bands at 3648 cm^{-1} and 1740 cm^{-1} were plotted against the concentration of the respective absorbing function in Fig. 9b and c. For both phenol and ester functions, a slope breaking was observed for a concentration around 1.6×10^{-2} mol L^{-1}. This change in slope is particularly abrupt for the phenol function. According to Beer-Lambert's law, the slope gives directly access to the molar extinction coefficient of the absorbing function. Thus, this slope breaking could be due to a change in the molar extinction coefficient.

As shown in Table 3, for concentrations of phenol or ester functions lower than 1.6×10^{-2} mol L^{-1}, the values of the corresponding molar extinction coefficients are consistent with those usually reported in the literature [43–45]. However, above this critical concentration, the molar extinction coefficients are considerably higher than expected.

An important point is that AO crystals started to be detected on the polymer film surface above almost the same critical concentration (Fig. 6b). Thus, a reasonable hypothesis could be that the observed changes in the molar extinction coefficients might be related to the appearance of AO crystals in Si-g-LLDPE films. Unfortunately, at this stage of investigation, no explanation was found on the fact that these coefficients are much higher than those found previously for the commercial Irganox 1076® powder (see Table 2).

Although there was no appearance of new bands in FTIR spectra, a broadening of the initial IR bands of phenol and ester functions in their low wavenumber domain was clearly observed, presumably due to the development of shoulders when increasing the AO concentration. These shoulders could be assigned to the formation of AO agglomerates or crystals in the polymer bulk or on the polymer film surface. Thus, the molar extinction coefficient determined for higher concentrations should rather be considered as a "composite" coefficient.

Results from literature showed that, for a given chemical bond, a wavenumber shift of the IR band towards lower values is generally associated with an increase of the molar extinction coefficient [46,60–62]. More particularly, it was reported in literature that, when their concentration is sufficiently high, polar species such as alcohols can be associated through H-bonding into series of *n*-mers [63–67]. This H-bonding is generally accompanied with a broadening and a shift towards lower wavenumbers of the IR absorption bands, but also with a change in the value of the corresponding molar extinction coefficient. Indeed, according to several authors, the molar extinction coefficient tends to increase with the formation of H-bonded agglomerates [64,67]. As an example, Martinez [64] studied a methanol/n-hexane system in which different types of agglomerates can be formed. This author found that the molar extinction coefficient of the O–H stretching band is higher for the agglomerates than for the monomer.

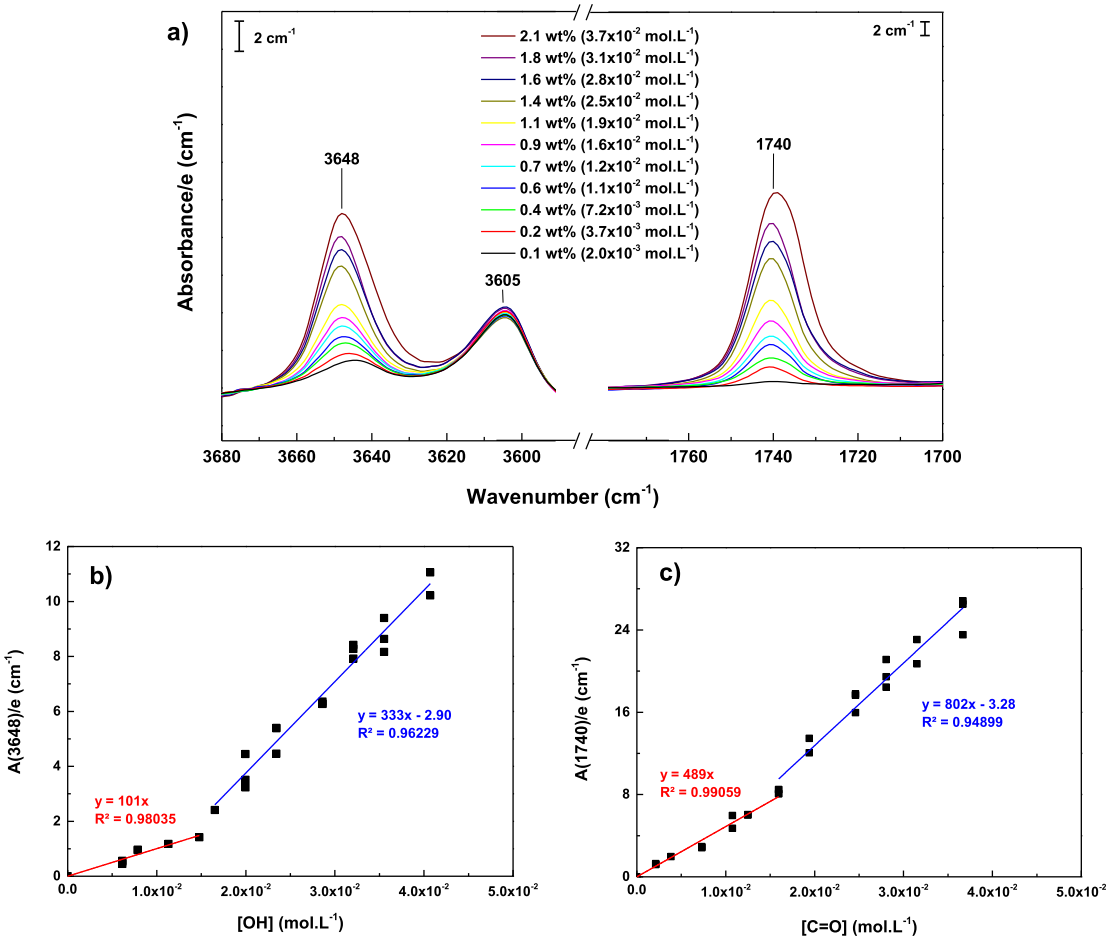

Fig. 9. a) Normalized hydroxyl and carbonyl regions of the FTIR spectra obtained in transmission mode for Si-g-LLDPE films stabilized with an increasing concentration in Irganox 1076®, b) Calibration curve of A (3648)/e against [OH], and c) Calibration curve of A (1740)/e against [C=O].

Table 3
Molar extinction coefficients obtained for phenol (OH) and ester (C=O) functions in Si-g-LLDPE films using FTIR spectroscopy in transmission mode. C is the concentration of the absorbing function under consideration.

FTIR	ε_{phenol} ($L.mol^{-1}.cm^{-1}$)	ε_{ester} ($L.mol^{-1}.cm^{-1}$)
$C \leq 1.6 \times 10^{-2}$ mol L^{-1}	101 ± 5	489 ± 12
$C \geq 1.6 \times 10^{-2}$ mol L^{-1}	333 ± 20	802 ± 50

Finally, Si-g-LLDPE films were characterized by DSC. The resulting DSC thermograms are overlaid in Fig. 10. An endothermic peak was observed around 51 °C for samples containing a minimal concentration in Irganox 1076® of 0.9 wt% ($\approx 1.6 \times 10^{-2}$ mol L^{-1}). This endothermic peak corresponds to the melting of the Irganox 1076® crystals and thus, is representative of the presence of insoluble Irganox 1076® crystals in the polymer bulk and/or on the polymer film surface. According to the previous DSC results obtained for the commercial Irganox 1076® powder (see Fig. 2), but also to the literature, this melting peak would be assigned to the crystalline form I of Irganox 1076®.

These DSC results are also consistent with the previous FTIR results, as antioxidant crystals were detected using FTIR spectroscopy in ATR mode above the same critical concentration.

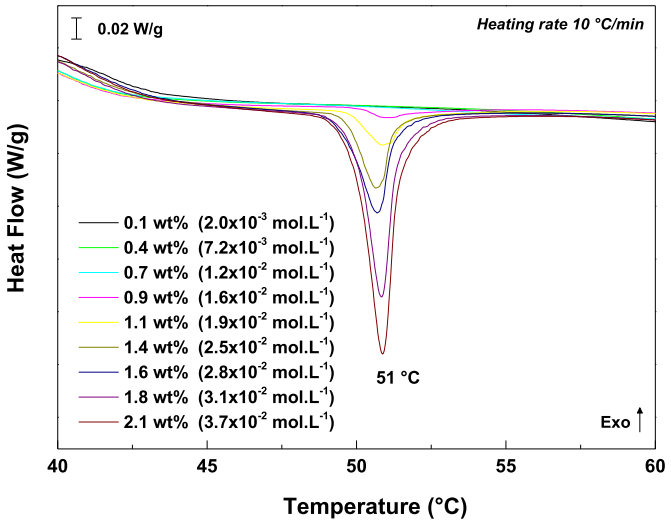

Fig. 10. DSC thermograms of Si-g-LLDPE films stabilized with an increasing concentration of Irganox 1076®.

3.2.2.2. Si-XLPE films. Si-XLPE film stabilized with at least 1 wt% ($\approx 1.7 \times 10^{-2}$ mol L^{-1}) of Irganox 1076® were also characterized by FTIR spectroscopy in transmission mode and DSC after one week of thermal treatment at 70 °C under vacuum in order to investigate the changes occurring in the polymer bulk.

The hydroxyl and carbonyl regions of the FTIR spectra obtained before and after thermal treatment, normalized with the thickness

of the polymer film, are given in Fig. 11.

Before thermal treatment, the IR bands of the phenol and the ester functions of AO were observed at 3642 cm^{-1} and 1736 cm^{-1}, respectively. This result indicates the presence of a large population of nodules of crystalline form I of Irganox 1076® in the polymer bulk. As a reminder, the IR band around 3605 cm^{-1} is assigned to PE [57–59].

Then, after thermal treatment, a slight shift of the two bands towards higher wavenumbers (at 3649 cm^{-1} and 1741 cm^{-1}, respectively) was observed. These new positions are characteristic to well dissolved Irganox 1076® in Si-XLPE film, as already evidenced in Si-g-LLDPE films. In addition to these slight shifts, the formation of two new IR bands was observed at 3610 cm^{-1} and 1724 cm^{-1}, respectively. These two bands are assigned to the crystalline form III Irganox 1076®, as previously monitored by FTIR spectroscopy in ATR mode. A shoulder of the ester band can be observed at 1736 cm^{-1}, meaning that AO crystals in their initial crystalline form are still present in the sample after thermal treatment, but in a much smaller concentration.

Thus, thermal treatment would lead to the following scenario: at 70 °C i.e., above their melting point (51 °C), the nodules of the crystalline form I of Irganox 1076® solubilize in the polymer bulk, and the AO molecules migrates up to the polymer film surface where they exude. Then, during cooling at room temperature, AO molecules recrystallize under form III on the polymer film surface, thus explaining the appearance of IR bands of form III at 3610 cm^{-1} and 1724 cm^{-1}. As a consequence, the polymer bulk considerably depletes in AO nodules, revealing finally the presence of well dissolved Irganox 1076® in Si-XLPE film with characteristic IR bands located at 3649 cm^{-1} and 1741 cm^{-1}.

Hence, these additional results are supporting the two previous hypotheses: i) The presence of different associations of AO molecules into crystalline structures in the polymer bulk, having slightly different positions of IR bands than dissociated AO molecules; ii) The presence of two crystalline structures (i.e. form I and form III) on the polymer film surface.

In addition to FTIR spectroscopy, DSC analysis was also performed on Si-XLPE film before and after thermal treatment, and the corresponding DSC thermograms are given in Fig. 12. As previously seen for Si-g-LLDPE films, a single endothermic peak is observed at 51 °C on the DSC thermograms of the untreated Si-XLPE film, which

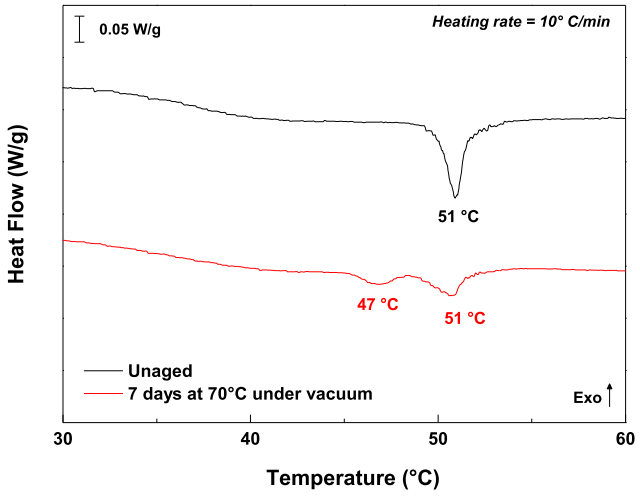

Fig. 12. DSC thermograms of the Si-XLPE film stabilized with Irganox 1076, before and after one week of thermal treatment at 70 °C under vacuum.

corresponds to the melting of the (crystalline) form I of Irganox 1076®. After thermal treatment, this endothermic peak is still observed but has decreased considerably in intensity and a smaller additional endothermic peak, at 47 °C, is observed. According to literature [33,41], this second endothermic peak corresponds to the melting of the (crystalline) form III of Irganox 1076®. These observations concord perfectly with the previous microscopic and FTIR analyses.

Thus, all experimental techniques used in this study confirm that Irganox 1076® is a molecule undergoing polymorphism and, according to literature, at least four different crystalline structure can exist [33,40,41]. However, at this stage of investigation, the preferential recrystallization of Irganox 1076® into the form III on the polymer surface is not very clear as many parameters can influence the recrystallization of a molecule into different possible structures (e.g., chemical environment, cooling conditions, thermal stability of each polymorph, etc.).

To conclude, as shown in this study, the polymorphism phenomenon leads to significant modifications of the physico-chemical

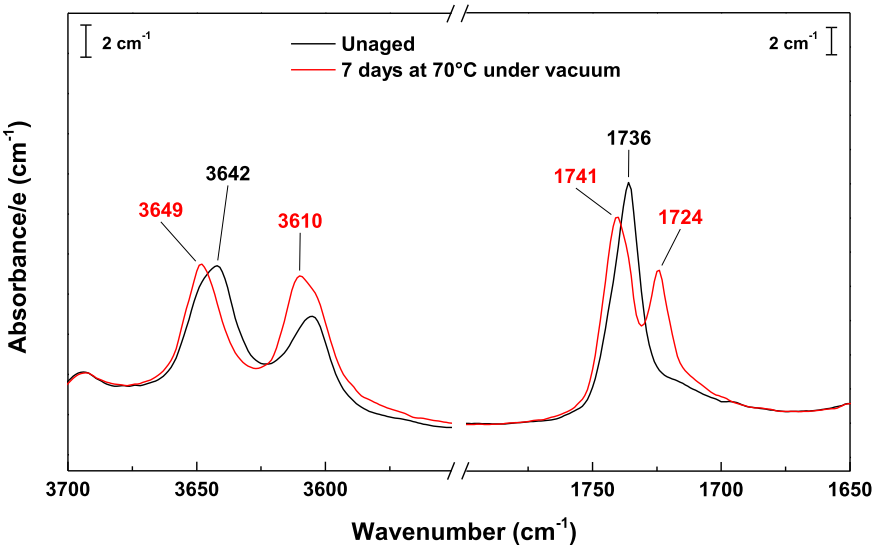

Fig. 11. Hydroxyl and carbonyl regions of the FTIR spectra obtained in transmission mode for the Si-XLPE film stabilized with Irganox 1076, before and after one week of thermal treatment at 70 °C under vacuum.

properties of antioxidants which could induce a misinterpretation of experimental results if not aware of this phenomenon. As an example, polymorphism leads to a significant shift of the IR absorption bands of antioxidants, which could be misinterpreted as the formation of oxidation products (such as hydroxyls and carbonyls) in the superficial layers of the polymer film and thus, by a poor resistance to oxidation of the material under study. Such a misinterpretation is expected to occur especially in relatively soft ageing conditions (i.e., a low temperature close to ambient), where oxidation reaction is generally very slow. Thus, the knowledge of this phenomenon and its kinetics appears to be crucial in any study on lifetime prediction.

3.3. Proposal of heterogeneous microstructural model

According to literature, and confirmed by our FTIR and DSC results, Irganox 1076® crystals in Si-g-LLDPE films seem to correspond to form I (i.e., the commercially available Irganox 1076® powder). Using the melting enthalpy of the Irganox 1076® crystal determined on the Irganox 1076® powder, it is possible to evaluate the concentration of insoluble AO in Si-g-LLDPE films using the following equation:

$$[\text{Irganox 1076}]_{\text{insol}} = \frac{\Delta H_{\text{m,Irganox 1076, film}}}{\Delta H_{\text{m, Irganox 1076, form I}}} \times \rho_{PE} \qquad \text{(Eq. 3)}$$

where ρ_{PE} is the polymer density ($0.918\ \text{g cm}^{-3}$), $\Delta H_{\text{m, Irganox 1076, form I}}$ the melting enthalpy of the crystalline form I of Irganox 1076® ($63.5\ \text{kJ mol}^{-1}$), and $\Delta H_{\text{m,Irganox 1076 film}}$ the melting enthalpy of the Irganox 1076® crystals in the stabilized Si-g-LLDPE film under study (J.g^{-1}).

Our FTIR and DSC results suggest that the antioxidant is present under two different physical states in Si-g-LLDPE film: totally dissolved in the polymer bulk (i.e. soluble AO) or under a crystalline structure (i.e. insoluble AO) in the polymer bulk and/or on the polymer film surface. Therefore, the total concentration in antioxidant can be written:

$$[\text{Irganox 1076}]_{\text{tot}} = [\text{Irganox 1076}]_{\text{sol}} + [\text{Irganox 1076}]_{\text{insol}} \qquad \text{(Eq. 4)}$$

Where $[\text{Irganox 1076}]_{\text{sol}}$ and $[\text{Irganox 1076}]_{\text{insol}}$ are the concentrations of the soluble and undissolved parts of Irganox 1076® in Si-g-LLDPE film, respectively.

As the concentration in insoluble Irganox 1076® can be determined from the melting enthalpy of AO crystals measured by DSC (Eq. (3)), the concentration in soluble Irganox 1076® can then be deduced by calculating the following difference: $[\text{Irganox 1076}]_{\text{tot}} - [\text{Irganox 1076}]_{\text{insol}}$. The resulting concentrations of both soluble and insoluble parts of Irganox 1076® were plotted against the total concentration in Irganox 1076 in Si-g-LLDPE films in Fig. 13. As expected, for $[\text{Irganox 1076}]_{\text{tot}} < 1.6 \times 10^{-2}\ \text{mol L}^{-1}$ (≈ 0.9 wt%), there is no formation of antioxidant crystals and thus, all antioxidants molecules are dissolved into the PE matrix. The concentration of soluble antioxidants is thus equal to $[\text{Irganox 1076}]_{\text{tot}}$. Then, for $[\text{Irganox 1076}]_{\text{tot}} \geq 1.6 \times 10^{-2}\ \text{mol L}^{-1}$, $[\text{Irganox 1076}]_{\text{sol}}$ reaches the asymptotic value of $1.6 \times 10^{-2}\ \text{mol L}^{-1}$, corresponding to the solubility threshold of Irganox 1076® in the PE matrix. The polymer matrix is fully saturated with antioxidants and only antioxidant crystals can be formed. Therefore, $[\text{Irganox 1076}]_{\text{insol}}$ starts to increase proportionally with $[\text{Irganox 1076}]_{\text{tot}}$.

According to all these results, the phase separation in the polymer bulk and the blooming of antioxidants onto the polymer film surface can schematically be represented as shown in Fig. 14.

When the concentration of antioxidants is below the solubility threshold $[\text{AO}]_c = 1.6 \times 10^{-2}\ \text{mol L}^{-1}$ (≈ 0.9 wt%), all antioxidants are solubilized in the polymer matrix. As the concentration of antioxidants increases up to reach $[\text{AO}]_c$, the polymer totally saturates in antioxidants. If more antioxidants are incorporated into the polymer matrix, the excess of antioxidant can no longer be dissolved and thus, a phase separation occurs leading to the formation of antioxidant crystals. In this latter case, there will be a heterogeneous distribution of antioxidants in the PE matrix leading to the formation and coexistence of two different phases: an AO-saturated polymer matrix plus antioxidant crystals within the polymer bulk and/or bloomed onto the polymer film surface.

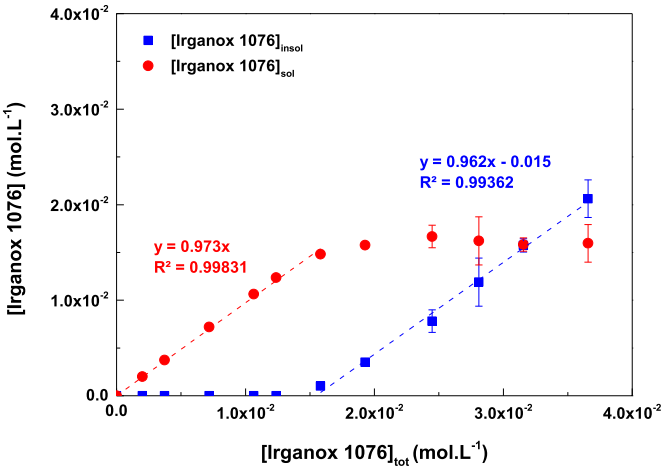

Fig. 13. Concentrations of insoluble and soluble parts of Irganox 1076® against total concentration of Irganox 1076® in Si-g-LLDPE films, determined by DSC.

During thermal ageing, the depletion of antioxidants is due to both the chemical consumption (through stabilization reactions) and physical loss of antioxidants [68,69]. In the case of the thermal treatment at 70 °C under vacuum, only physical loss occurs as illustrated in Fig. 15. In the case of a heterogeneous distribution of antioxidants, as proposed previously, a first assumption is that, during thermal ageing, only the dissolved AO are chemically consumed and exudate on the polymer film surface. On the other hand, the undissolved crystalline AO phase are considered to act as a "reservoir" of AO. As the dissolved AO concentration decreases, the AO crystals in the polymer bulk solubilize in order to maintain constant the concentration of soluble. In other words, only the concentration of AO nodules decreases in the polymer bulk. In addition, as AO exudates at the surface, an increase of AO crystals is likely to occur at the polymer film surface, with potentially recrystallization into different crystalline structures.

4. Conclusion

In this study, the exudation and blooming of Irganox 1076® onto the surface of polyethylene-based materials was investigated. Physico-chemical characterization techniques, such as FTIR spectroscopy and DSC, were used to detect the formation of Irganox 1076® crystals. In particular, a solubility threshold of 0.9 wt% ($\approx 1.6 \times 10^{-2}\ \text{mol L}^{-1}$) was determined for Irganox 1076® in the PE matrix. This value corresponds to the critical concentration of antioxidants above which a phase separation is detected. In addition, these techniques were used to determine the concentration of both soluble and undissolved parts of antioxidant in the PE matrix.

This methodology was then applied to a Si-XLPE film containing at least 1 wt% of Irganox 1076® as in-service protective antioxidant. FTIR spectroscopy and DSC were also found very useful to detect the polymorphism phenomenon of Irganox 1076®. Indeed, after a

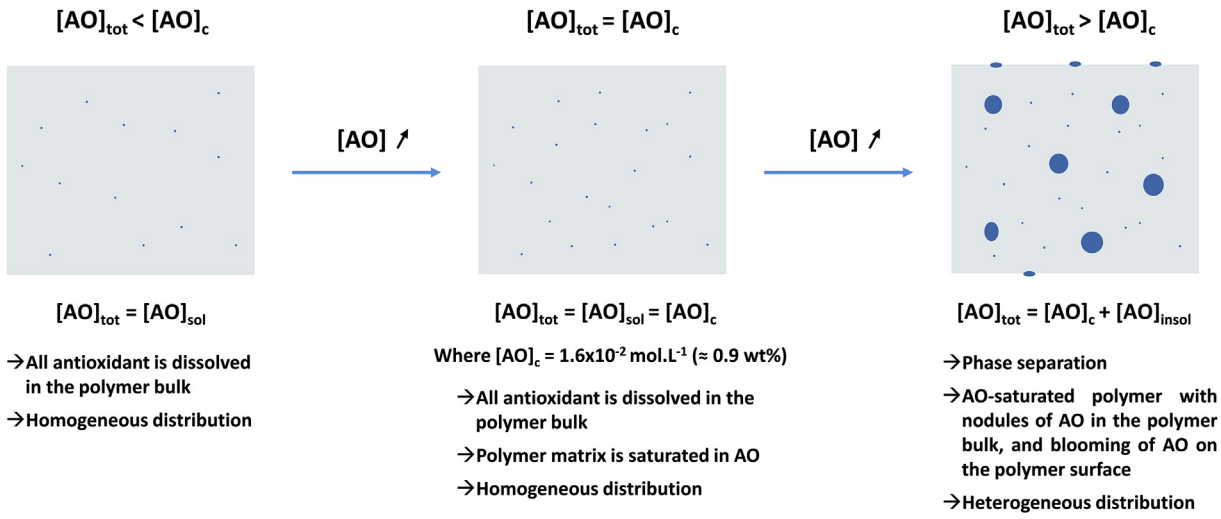

Fig. 14. Schematic representation of phase separation with blooming of antioxidants onto the polymer film surface. $[AO]_c$ is the solubility threshold of AO in the PE matrix, above which a phase separation occurs.

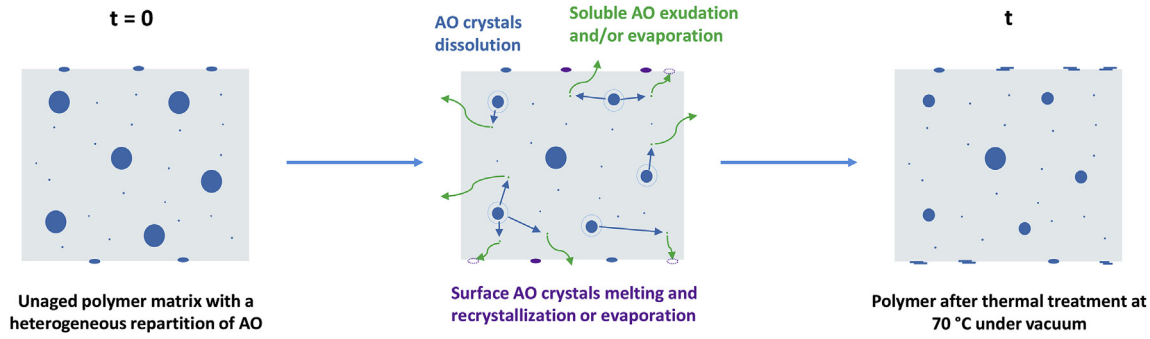

Fig. 15. Schematic representation of the physical phenomena which could occur during the thermal treatment at 70 °C under vacuum of a heterogeneously stabilized polymer.

thermal treatment above the melting point of Irganox 1076® under vacuum, new needle-shaped crystals were observed onto the polymer film surface with optical microscopy. The transformation of the (crystalline) form I of Irganox 1076® into the (crystalline) form III leads to a shift of the IR absorption bands of both phenol and ester functions towards lower wavenumbers (typically from 3639 to 3612 cm^{-1} and from 1733 to 1723 cm^{-1}, respectively) in the FTIR spectra obtained in ATR mode, but also the appearance of a new melting peak at 47 °C on the DSC thermograms.

In future works, these techniques will be also used to detect the polymorphism phenomenon of antioxidants during the thermal and radiochemical ageing of polyethylene-based materials. As polymorphism leads to significant modifications of the physico-chemical properties of antioxidants, it will be important to take into account this phenomenon when analysing the experimental results in order to avoid misinterpretations, in particular, of FTIR results. A challenge will be to (chemically or mathematically) deconvoluate the formation of new hydroxyl and carbonyl products, for instance generated by the oxidative degradation of the polymer, from the unceasing reorganization of antioxidant molecules in the polymer bulk and/or on the polymer sample surface.

A further question will be the consequence of such a heterogeneous distribution of antioxidants in the polymer bulk and/or on the polymer sample surface on the efficiency of the polymer stabilization. As mentioned, an assumption could be that, during oxidative ageing, only the dissolved part of antioxidants stabilizes the polymer matrix, while the pure AO phase (in excess) acts as a "reservoir", i.e. maintaining constant the concentration of dissolved antioxidants at its solubility threshold in the PE matrix during the early periods of ageing. Of course, this "reservoir" effect will completely disappear with the excess of antioxidants. In such a model, the stabilization efficiency would thus be proportional to the concentration of dissolved antioxidants, but could be considerably improved by increasing the "volume of the reservoir".

Author contributions section

Anne Xu: Methodology, Investigation, Conceptualization, Writing- Original Draft. Sébastien Roland.: Validation, Writing- Review & Editing. Xavier Colin: Validation, Writing- Review & Editing, Supervision.

Declaration of competinf interest

The authors declare that they have no known competing financial interests or personal relationships that could have appeared to influence the work reported in this paper.

Acknowledgments

This research is part of the European Project "TeaM Cables" aimed at providing to nuclear power plants (NPP) operators a novel methodology for a more efficient and reliable management of the electrical cables ageing, in particular by developing specific

experimental and kinetic modelling tools.

The project leading to this application has received funding from the Euratom research and training program 2014–2018 under grant agreement No 755183.

References

[1] G.L. Oliveira, M.F. Costa, Optimization of process conditions, characterization and mechanical properties of silane crosslinked high-density polyethylene, Mater. Sci. Eng., A 527 (2010) 4593–4599, https://doi.org/10.1016/j.msea.2010.03.102.

[2] S.M. Tamboli, S.T. Mhaske, D.D. Kale, Crosslinked polyethylene, Indian J. Chem. Technol. 11 (2004) 853–864.

[3] Y.-T. Shieh, C.-M. Liu, Silane grafting reactions of LDPE, HDPE, and LLDPE, J. Appl. Polym. Sci. 74 (1999) 3404–3411, https://doi.org/10.1002/(SICI)1097-4628(19991227)74:14<3404::AID-APP14>3.0.CO;2-S.

[4] G.B. Shah, M. Fuzail, J. Anwar, Aspects of the crosslinking of polyethylene with vinyl silane, J. Appl. Polym. Sci. 92 (2004) 3796–3803, https://doi.org/10.1002/app.20381.

[5] J. Morshedian, P.M. Hosseinpour, Polyethylene cross-linking by two-step silane method: a Review, Iran. Polym. J. (Engl. Ed.) 18 (2009) 103–128.

[6] J.E. Mark, Physical Properties of Polymers Handbook, Springer Science & Business Media, 2007.

[7] C. Vasile, M. Pascu, Practical Guide to Polyethylene, iSmithers Rapra Publishing, 2005.

[8] H. Dodiuk, S.H. Goodman, Handbook of Thermoset Plastics, Elsevier, 1999.

[9] G. Pritchard, Plastics Additives: an A-Z Reference, Springer Science & Business Media, 2012.

[10] Miroslav Pastorek, Crosslinking and Ageing of Ethylene-Vinyl Silane Copolymers, Tomas Bata University, 2014.

[11] Y.-T. Shieh, T.-H. Tsai, Silane grafting reactions of low-density polyethylene, J. Appl. Polym. Sci. 69 (1998) 255–261, https://doi.org/10.1002/(SICI)1097-4628(19980711)69:2<255::AID-APP6>3.0.CO;2-M.

[12] X. Colin, B. Fayolle, L. Audouin, J. Verdu, About a quasi-universal character of unstabilised polyethylene thermal oxidation kinetics, Polym. Degrad. Stab. 80 (2003) 67–74, https://doi.org/10.1016/S0141-3910(02)00384-1.

[13] X. Colin, L. Audouin, J. Verdu, Determination of thermal oxidation rate constants by an inverse method. Application to polyethylene, Polym. Degrad. Stab. 86 (2004) 309–321, https://doi.org/10.1016/j.polymdegradstab.2004.04.022.

[14] N. Khelidj, X. Colin, L. Audouin, J. Verdu, C. Monchy-Leroy, V. Prunier, Oxidation of polyethylene under irradiation at low temperature and low dose rate. Part II. Low temperature thermal oxidation, Polym. Degrad. Stab. 91 (2006) 1598–1605, https://doi.org/10.1016/j.polymdegradstab.2005.09.012.

[15] X. Colin, B. Fayolle, L. Audouin, J. Verdu, The classical kinetic model for radical chain oxidation of hydrocarbon substrates initiated by bimolecular hydroperoxide decomposition, Int. J. Chem. Kinet. 38 (2006) 666–676, https://doi.org/10.1002/kin.20201.

[16] E. Richaud, X. Colin, B. Fayolle, L. Audouin, J. Verdu, Induction period in the low-temperature thermal oxidation of saturated hydrocarbons: example of polyethylene, Int. J. Chem. Kinet. 40 (2008) 769–777, https://doi.org/10.1002/kin.20347.

[17] N. Khelidj, X. Colin, L. Audouin, J. Verdu, A simplified approach for the lifetime prediction of PE in nuclear environments, Nucl. Instrum. Methods Phys. Res. Sect. B Beam Interact. Mater. Atoms 236 (2005) 88–94, https://doi.org/10.1016/j.nimb.2005.03.259.

[18] N. Khelidj, X. Colin, L. Audouin, J. Verdu, C. Monchy-Leroy, V. Prunier, Oxidation of polyethylene under irradiation at low temperature and low dose rate. Part I. The case of “pure” radiochemical initiation, Polym. Degrad. Stab. 91 (2006) 1593–1597, https://doi.org/10.1016/j.polymdegradstab.2005.09.011.

[19] X. Colin, C. Monchy-Leroy, L. Audouin, J. Verdu, Lifetime prediction of polyethylene in nuclear plants, Nucl. Instrum. Methods Phys. Res. Sect. B Beam Interact. Mater. Atoms 265 (2007) 251–255, https://doi.org/10.1016/j.nimb.2007.08.086.

[20] X. Colin, E. Richaud, J. Verdu, C. Monchy-Leroy, Kinetic modelling of radiochemical ageing of ethylene–propylene copolymers, Radiat. Phys. Chem. 79 (2010) 365–370, https://doi.org/10.1016/j.radphyschem.2009.08.019.

[21] J. Verdu, X. Colin, B. Fayolle, L. Audouin, Methodology of lifetime prediction in polymer ageing, JTE 35 (2007) 289–296, https://doi.org/10.1520/JTE100477.

[22] A. François-Heude, E. Richaud, E. Desnoux, X. Colin, Influence of temperature, UV-light wavelength and intensity on polypropylene photothermal oxidation, Polym. Degrad. Stab. 100 (2014) 10–20, https://doi.org/10.1016/j.polymdegradstab.2013.12.038.

[23] A. François-Heude, E. Richaud, E. Desnoux, X. Colin, A general kinetic model for the photothermal oxidation of polypropylene, J. Photochem. Photobiol. A Chem. 296 (2015) 48–65, https://doi.org/10.1016/j.jphotochem.2014.08.015.

[24] X. Colin, L. Audouin, J. Verdu, M. Rozental-Evesque, B. Rabaud, F. Martin, F. Bourgine, Ageing of polyethylene pipes transporting drinking water disinfected by chlorine dioxide. I. Chemical aspects, Polym. Eng. Sci. 49 (2009) 1429–1437, https://doi.org/10.1002/pen.21258.

[25] X. Colin, L. Audouin, J. Verdu, M. Rozental-Evesque, B. Rabaud, F. Martin, F. Bourgine, Ageing of polyethylene pipes transporting drinking water disinfected by chlorine dioxide. Part II—lifetime prediction, Polym. Eng. Sci. 49 (2009) 1642–1652, https://doi.org/10.1002/pen.21387.

[26] X. Colin, L. Audouin, J. Verdu, Towards a Non Empirical Kinetic Model for the Lifetime Prediction of Polyethylene Pipes Transporting Drinking Water, vol. 286, Macromolecular Symposia, 2009, pp. 81–88, https://doi.org/10.1002/masy.200951210.

[27] A. Mikdam, X. Colin, G. Minard, N. Billon, R. Maurin, A kinetic model for predicting the oxidative degradation of additive free polyethylene in bleach desinfected water, Polym. Degrad. Stab. 146 (2017) 78–94, https://doi.org/10.1016/j.polymdegradstab.2017.09.020.

[28] T. Seguchi, K. Tamura, A. Shimada, M. Sugimoto, H. Kudoh, Mechanism of antioxidant interaction on polymer oxidation by thermal and radiation ageing, Radiat. Phys. Chem. 81 (2012) 1747–1751, https://doi.org/10.1016/j.radphyschem.2012.06.011.

[29] S. Al-Malaika, S. Riasat, C. Lewucha, Reactive antioxidants for peroxide crosslinked polyethylene, Polym. Degrad. Stab. 145 (2017) 11–24, https://doi.org/10.1016/j.polymdegradstab.2017.04.013.

[30] S. Al-Malaika, Perspectives in stabilisation of polyolefins, in: A.-C. Albertsson (Ed.), Long Term Properties of Polyolefins, Springer Berlin Heidelberg, Berlin, Heidelberg, 2004, pp. 121–150, https://doi.org/10.1007/b13521.

[31] X. Colin, B. Fayolle, L. Audouin, J. Verdu, Phénomènes de transport des stabilisants dans les polyoléfines - partie II : solubilité, Matériaux Tech. 91 (2003) 9–14, https://doi.org/10.1051/mattech/200391010009.

[32] H.E. Bair, Exudation of an antioxidant additive from thin polyethylene films, Polym. Eng. Sci. 13 (1973) 435–439, https://doi.org/10.1002/pen.760130607.

[33] J. Saunier, V. Mazel, C. Paris, N. Yagoubi, Polymorphism of Irganox 1076®: discovery of new forms and direct characterization of the polymorphs on a medical device by Raman microspectroscopy, Eur. J. Pharm. Biopharm. 75 (2010) 443–450, https://doi.org/10.1016/j.ejpb.2010.04.014.

[34] N. Médard, A. Benninghoven, D. Rading, A. Licciardello, A. Auditore, T.M. Duc, H. Montigaud, F. Vernerey, C. Poleunis, P. Bertrand, Antioxidant segregation and crystallisation at polyester surfaces studied by ToF-SIMS, Appl. Surf. Sci. 203–204 (2003) 571–574, https://doi.org/10.1016/S0169-4332(02)00768-7.

[35] R. Spatafore, L.T. Pearson, Migration and blooming of stabilizing antioxidants in polypropylene, Polym. Eng. Sci. 31 (1991) 1610–1617, https://doi.org/10.1002/pen.760312209.

[36] T.G. RYAN, P.D. CALVERT, N.C. BILLINGHAM, The distribution of additives and impurities in isotactic polypropylene, in: Stabilization and Degradation of Polymers, American Chemical Society, 1978, pp. 261–272, https://doi.org/10.1021/ba-1978-0169.ch022.

[37] J. Saunier, V. Mazel, C. Aymes-Chodur, N. Yagoubi, Blooming of Irganox 3114® antioxidant onto a medical grade elastomer. Impact of the recrystallization conditions on the antioxidant polymorphism, on the film wettability and on the antioxidant leachability, Int. J. Pharm. 437 (2012) 89–99, https://doi.org/10.1016/j.ijpharm.2012.07.060.

[38] A. Burger, R. Ramberger, On the polymorphism of pharmaceuticals and other molecular crystals. I, Mikrochim. Acta 72 (1979) 259–271, https://doi.org/10.1007/BF01197379.

[39] A. Burger, R. Ramberger, On the polymorphism of pharmaceuticals and other molecular crystals. II, Mikrochim. Acta 72 (1979) 273–316, https://doi.org/10.1007/BF01197380.

[40] K. Molt, D. Ihlbrock, Principles and applications of quality control by near infrared spectroscopy using the example of polymer additives, Fresenius J. Anal. Chem. 348 (1994) 523–529, https://doi.org/10.1007/BF00323923.

[41] J. Saunier, J.-M. Herry, N. Yagoubi, C. Marlière, Exploring complex transitions between polymorphs on a small scale by coupling AFM, FTIR and DSC: the case of Irganox 1076® antioxidant, RSC Adv. 7 (2017) 3804–3818, https://doi.org/10.1039/C6RA25632E.

[42] B.H. Stuart, Infrared Spectroscopy: Fundamentals and Applications, John Wiley & Sons, 2004.

[43] N. Khelidj, Vieillissement d’isolants de câbles en polyéthylène en ambiance nucléaire, ENSAM, Paris, 2006. http://www.theses.fr/2006ENAM0033. (Accessed 16 February 2018).

[44] M. St, G. Flett, Intensities of some group characteristic infra-red bands, Spectrochim. Acta 18 (1962) 1537–1556, https://doi.org/10.1016/0371-1951(62)80018-6.

[45] J. Tireau, Proprietes a long terme des gaines de polyethylene haute densite utilisees pour les ponts a haubans, phdthesis, Arts et Métiers ParisTech, 2011, https://pastel.archives-ouvertes.fr/pastel-00562683/document. (Accessed 17 January 2019).

[46] H.L. McMurry, V. Thornton, Correlation of infrared spectra, Anal. Chem. 24 (1952) 318–334, https://doi.org/10.1021/ac60062a018.

[47] D.J. Carlsson, D.M. Wiles, The photodegradation of polypropylene films. III. Photolysis of polypropylene hydroperoxides, Macromolecules 2 (1969) 597–606, https://doi.org/10.1021/ma60012a007.

[48] D.W. van Krevelen, K. te Nijenhuis, Properties of Polymers: Their Correlation with Chemical Structure; Their Numerical Estimation and Prediction from Additive Group Contributions, Elsevier, 2009.

[49] Q. Gu, C. Trindle, J.L. Knee, Communication: frequency shifts of an intramolecular hydrogen bond as a measure of intermolecular hydrogen bond strengths, J. Chem. Phys. 137 (2012), https://doi.org/10.1063/1.4752246, 091101.
[50] P. Pagès, Characterization of Polymer Materials Using FT-IR and DSC Techniques, Universidade da Coruña, 2005. http://ruc.udc.es/dspace/handle/2183/11499. (Accessed 25 April 2019).
[51] N.J. Harrick, Study of physics and chemistry of surfaces from frustrated total internal reflections, Phys. Rev. Lett. 4 (1960) 224–226, https://doi.org/10.1103/PhysRevLett.4.224.
[52] S. Swathi, S. Srikanth, V.U.M. Rao, Attenuated total reflectance spectroscopy, Overview 4 (2014) 8.
[53] C. Vasile, Handbook of Polyolefins, CRC Press, 2000.
[54] G. Wypych, Handbook of Polymers, Elsevier, 2016.
[55] D.R. Smith, E.V. Loewenstein, Optical constants of far infrared materials. 3: plastics, Appl. Opt., AO. 14 (1975) 1335–1341, https://doi.org/10.1364/AO.14.001335.
[56] Bruker optics, Attenuated Total Reflection (ATR) – a versatile tool for FT-IR spectroscopy, Appl. Note AN 79 (2011).
[57] J.R. Nielsen, A.H. Woollett, Vibrational spectra of polyethylenes and related substances, J. Chem. Phys. 26 (1957) 1391–1400, https://doi.org/10.1063/1.1743551.
[58] B. Peters, S.L. Scott, A. Fong, Y. Wang, A.E. Stiegman, Reexamining the evidence for proton transfers in ethylene polymerization, Proc. Natl. Acad. Sci. 112 (2015) E4160–E4161, https://doi.org/10.1073/pnas.1422589112.
[59] J. Rud Nielsen, R.F. Holland, Dichroism and interpretation of the infrared bands of oriented crystalline polyethylene, J. Mol. Spectrosc. 6 (1961) 394–418, https://doi.org/10.1016/0022-2852(61)90264-8.
[60] V.A. Matyshak, O.V. Krylov, Problems of quantitative spectroscopic measurements in heterogeneous catalysis: molar absorption coefficients of vibrations in adsorbed substances, Kinet. Catal. 43 (2002) 391–407, https://doi.org/10.1023/A:1016066120097.
[61] A. Barth, Infrared spectroscopy of proteins, Biochim. Biophys. Acta Bioenerg. 1767 (2007) 1073–1101, https://doi.org/10.1016/j.bbabio.2007.06.004.
[62] M. Koch-Müller, D. Rhede, IR absorption coefficients for water in nominally anhydrous high-pressure minerals, Am. Mineral. 95 (2010) 770–775.
[63] Y. Liu, M.A. Czarnecki, Y. Ozaki, M. Suzuki, M. Iwahashi, Determination of the molar absorption coefficient for the second overtone of an OH stretching mode of Z-9-otadecen-1-ol, Vib. Spectrosc. 9 (1995) 221–224, https://doi.org/10.1016/0924-2031(94)00088-X.
[64] S. Martinez, Methanol/n-hexane system—I. Infrared studies, Spectrochim. Acta 42 (1986) 531–536, https://doi.org/10.1016/0584-8539(86)80050-2.
[65] A.N. Fletcher, C.A. Heller, Self-association of alcohols in nonpolar solvents | the journal of physical chemistry, J. Phys. Chem. 71 (1967) 3742–3756, https://doi.org/10.1021/j100871a005.
[66] F. Franks, D.J.G. Ives, The structural properties of alcohol–water mixtures, Q. Rev. Chem. Soc. 20 (1966) 1–44, https://doi.org/10.1039/QR9662000001.
[67] G.C. Pimentel, A.L. McClellan, The Hydrogen Bond, W. H. Freeman And Company, 1960. https://archive.org/details/hydrogenbond031051mbp/page/n9. (Accessed 8 July 2019).
[68] E. Richaud, C. Monchy-Leroy, X. Colin, L. Audouin, J. Verdu, Kinetic modelling of stabilization coupled with stabilizer loss by evaporation. Case of dithioester stabilized polyethylene, Polym. Degrad. Stab. 94 (2009) 2004–2014, https://doi.org/10.1016/j.polymdegradstab.2009.07.017.
[69] E. Richaud, J. Verdu, Vieillissement chimique des polymères Physicochimie de la stabilisation, Techniques de l'ingénieur Propriétés Générales Des Plastiques. base documentaire , TIB152DUO, https://www.techniques-ingenieur.fr/base-documentaire/materiaux-th11/proprietes-generales-des-plastiques-42152210/vieillissement-chimique-des-polymeres-am3153/, 2012.